Discharge Directionality and Dominance of Right-Handed Modes in Helicon Plasmas due to Radial Electron Density Gradients

Marcel Granetzny Oliver Schmitz, and Michael Zepp
University of Wisconsin - Madison, Department of Engineering Physics, WI, USA
(Dated: December 23, 2022)

Helicon waves are magnetized plasma waves, similar to whistler waves in Earth's ionosphere, that are used to create high-density laboratory plasmas. We demonstrate that the discharge direction can be reversed by changing the antenna helicity or the magnetic field direction. Simulations reproduce these findings if a radial density gradient exists. A helicon wave equation that includes such a density gradient gives rise to a modulating magnetic field that amplifies right-handed but attenuates left-handed helicon modes. This explains for the first time consistently the dominance of right-handed over left-handed modes and the discharge directionality in helicon plasmas.

Keywords: helicon, plasma, waves, direction, right-handed

Introduction Helicon waves 1 2 were discovered in the 1960s 3-6 and found to be in essence bounded whistler waves, similar to the ones propagating through Earth's ionosphere. As such they represent electromagnetic radio-frequency (RF) waves, typically at tens of MHz, in a bounded magnetized plasma. Their ability to excite steady-state high density plasmas 1, with reported densities reaching the 10^{20} m⁻³ range $\overline{7}$, directly from a cold gas is of interest to multiple fields of science and engineering including semiconductor-etching 8, advanced space propulsion 9, nuclear fusion materials testing 10, 11 and plasma wakefield acceleration 7. Soon after the discovery of helicon waves different antenna concepts were tested and significant differences were found in the achievable plasma generation efficiency. The leading concepts today are the Nagoya-III 12 and the half-helical (HH) 13 antennas. It was found that half-helical antennas produce the highest plasma density and induce a strong discharge directionality as evidenced by much higher density and temperature on one side of the antenna than the other 14.

Fig. 1 shows a right-handed (RH) half-helical antenna and the axial launch directions for modes with positive and negative azimuthal wave numbers, e.g. m = +1 and m = -1. A left-handed (LH) antenna reverses those launch directions. In helicon plasmas right- or lefthandedness of azimuthal modes can be uniquely defined relative to the background magnetic field direction. For example for the HH antenna in Fig. 1, the positive m modes rotate in the $\hat{\phi}$ direction while the negative m modes rotate in the opposite direction. For a magnetic background field pointing along \hat{z} this would make positive m modes right-handed and negative m modes left-handed. Over the years numerous groups have studied HH antennas with RH and LH helicity. It was found that right-handed helicon modes are measurably stronger than left-handed modes in terms of measured wavefields and that RH antennas produce higher plasma densities throughout the discharge than LH antennas,

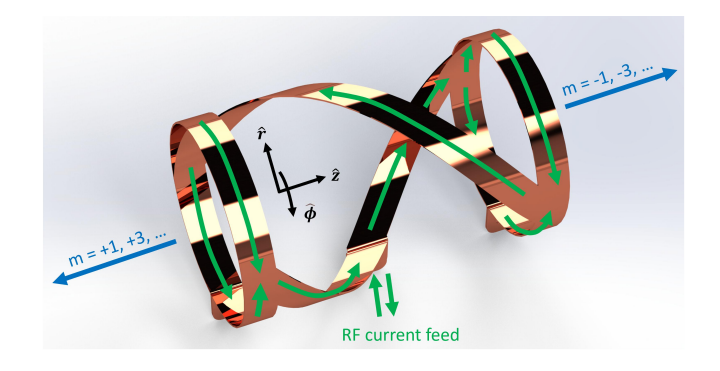


FIG. 1. Right-handed half-helical antenna. Currents during one half of the RF cycle are shown in green, the cylindrical coordinate system in black and launch directions for the different azimuthal modes in blue.

for reasons so far unknown 14, 15.

However, all those studies have been performed in experiments with complicating effects due to the vacuum vessel or magnetic field geometry. The most common case is the excitation of the helicon wave close to the axial boundary of the vacuum vessel, e.g. in 3, 13, 14, 16, 20, which introduces axially asymmetric boundary conditions around the antenna and can lead to discharges being launched directly into an axial boundary. In addition many experiments employ expansion chambers downstream of the helicon plasma creation region 21+25, resulting in strong axial density gradients. Another common setup features strong gradients in the axial magnetic field 22, 25–28. Inferring the reasons for the observed axial helicon discharge directionality and preference of right-handed modes is difficult in these setups because the helicon dispersion relation depends strongly on the magnetic field and density. To our knowledge no experimental study of the discharge directionality has been performed in a setup without these complicating effects. For the experiments presented here we generated the helicon discharge from the center of

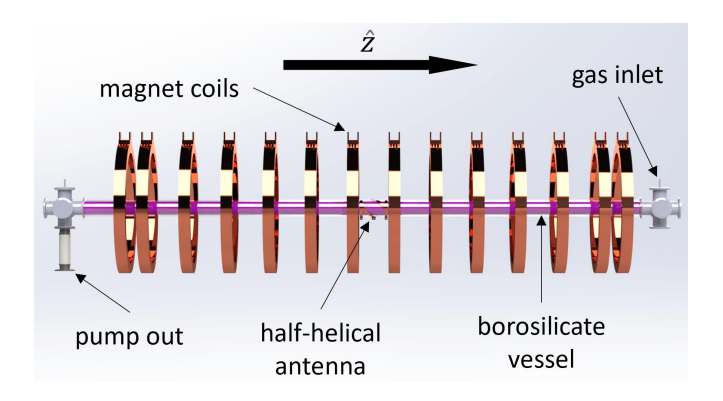


FIG. 2. CAD model of the core components of the MAP experiment.

a long vacuum vessel, with significant distance to both axial boundaries, and inside a highly homogeneous field. We documented the discharge features in detail and reproduced the experiments computationally using a quasi-3D finite element model.

Experiment The experiments presented here were performed at the Madison Awake Prototype (MAP), shown in Fig. 2 MAP consists of a 2 m long borosilicate glass tube with an ID of 52 mm and an OD of 58 mm. 14 coils produce a very homogeneous magnetic field of 49 mT in the central 1.6 m of the device, reaching 55 mT at the ends. The field can be directed either leftward or rightward in Fig. 2 A 10 cm long antenna with 1 cm wide straps is wound in either an RH or LH sense and used to excite the helicon plasma. The antenna is located at the center of the experiment at axial position z=0. All experiments were performed at an Argon fill pressure of 10^{-2} mbar with RF power input set to 1.3 kW at 13.56 MHz. An impedance matching network was used to reduce reflected power to negligible levels of less than 10 W. Gas was let in on the right side and forced to pass through the vacuum vessel before reaching the turbo pump on the left.

The plasma density was measured by means of laser-induced fluorescence (LIF) on singly ionized argon as described in [17] [29]. In addition photographs of the discharge around the antenna were taken. The results are shown in Fig. [3]. An RH antenna in a rightward magnetic field generates a leftward discharge (blue curve) while a leftward field yields a rightward discharge (green curve). The density profiles are mirrored around the antenna location. For an LH antenna the discharge is to the right for a rightward field (yellow) and to the left for a leftward field (red). This shows that reversal of either the antenna helicity or background field direction reverses the discharge direction and reversal of both restores the original discharge direction. The

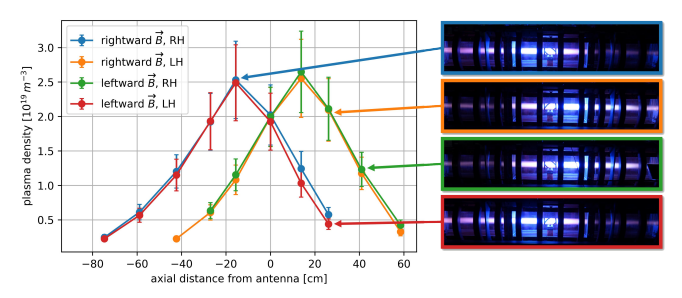


FIG. 3. Dependence of the helicon plasma density and light emission on the antenna helicity and magnetic field direction.

matching network was able to match all four plasmas without any adjustments which shows that the plasma impedance was identical across all discharges. These results, obtained with very good axial magnetic field homogeneity and proper distance to vacuum elements that could cause axial anisotropies, remove ambiguities in the experimental interpretation of other groups due to experimental setups, e.g. by placing the antenna towards a close-by axial boundary or regions with plasma density or field strength outside the values allowed by the dispersion relation 30.

Simulations Helicon discharges in MAP were modelled using a quasi-3D finite element code developed in COMSOL using the cold plasma wave description. In a high density helicon plasma a significant part of the power is deposited by the Trivelpiece-Gould 31 mode which has very short radial wavelength on the sub-mm scale. This necessitates use of very fine mesh elements of 500 μ m axially and 30 μ m radially. The model assumes that wavefields have an $e^{im\phi}$ dependence in the azimuthal direction, with m being the azimuthal mode number. Due to the strong damping of higher order modes, a full 3D solution can be calculated from the six leading order modes, namely $m = \{\pm 1, \pm 3, \pm 5\}$ as will be shown later in Fig. 5. Power deposition is calculated strictly ohmically through electron-ion and electron-neutral collisions since Landau damping is negligible 32. The model was verified by comparing results in a homogeneous plasma against the analytical helicon dispersion relation 30.

Density profiles for an RH antenna in a leftward field were measured at 116 points using the LIF technique. Plasma temperature and neutral pressure were set to be uniform at 3 eV and 10^{-3} mbar, respectively, the latter assuming a 90% neutral depletion. The results of this simulation are shown in Figs. 4 and 5 Fig. 4 shows the magnitude of the total wave magnetic field, with plasma density indicated by the white contour lines. The helicon wave propagates radially inwards and axially forward from the antenna location. Fig. 5 shows

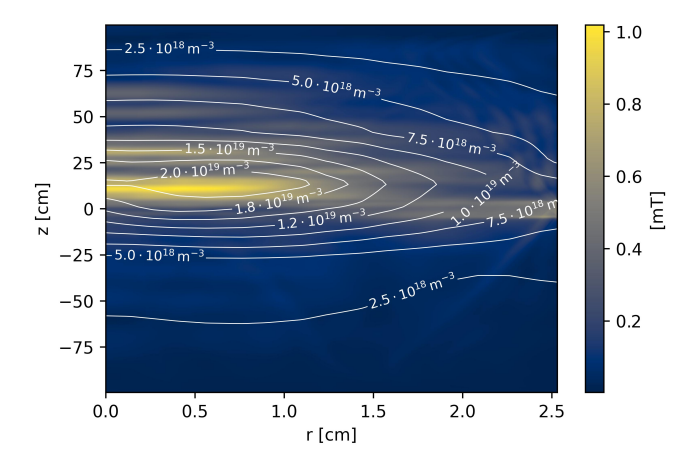


FIG. 4. Simulations results for total helicon wave magnetic field amplitude from an RH antenna with magnetic field in the negative z direction. Experimentally measured density given by white contour lines.

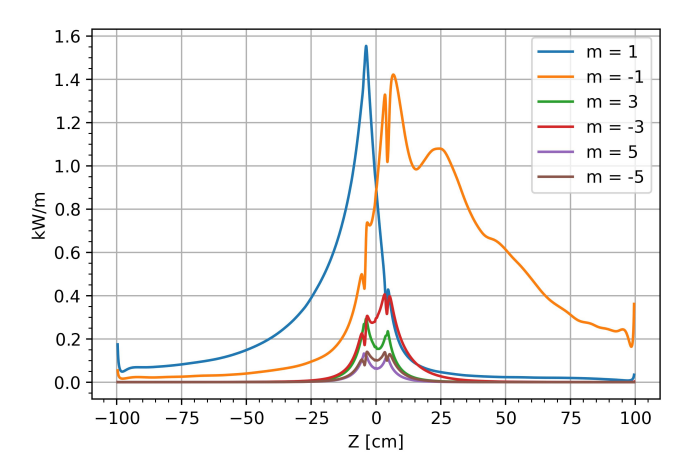


FIG. 5. Axial power deposition by azimuthal mode for the simulation in Fig. $\boxed{4}$

the radially integrated power deposition contributions from the different azimuthal modes. It is clear that the negative and positive m modes deposit power forwards and backwards, respectively, as expected from Fig. $\boxed{1}$ In this setup the dominant right-handed mode, m=-1, deposits 58.7% of the total power, mostly to the right. The leading left-handed mode, m=+1, deposits 29.5% of the total power, mostly in the opposite direction. The remaining 11.8% are accounted for by higher order modes which follow the directionality pattern of the leading RH and LH modes. Overall the power deposition is located in the discharge direction as observed optically and by LIF.

To shed light on the reason for this directional power deposition we performed simulations with axially uniform plasma density profiles. The radial plasma density profiles were either modelled as a flat top of the form [33]

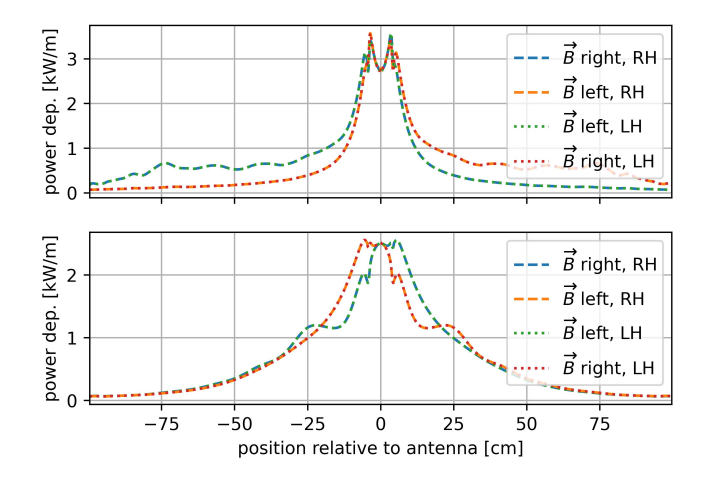


FIG. 6. Simulated power deposition profiles for helicon discharges in an axially uniform plasma with different field directions and antenna helicities. Top: With radial density gradient. Bottom: With radially uniform plasma. Blue and red as well as yellow and green traces are overlapping, respectively.

$$n_e = \left(n_e^{peak} - n_e^{edge}\right) \left(1 - \left(\frac{r}{r_w}\right)^5\right)^5 + n_e^{edge}, \quad (1)$$

with $n_e^{peak}=2.5\cdot 10^{19}~\mathrm{m}^{-3},\, n_e^{edge}=5.0\cdot 10^{18}~\mathrm{m}^{-3}$ and vacuum wall location $r_w=26~\mathrm{mm}$ or with a constant density of $n_e=2.5\cdot 10^{19}~\mathrm{m}^{-3}$ throughout.

Results for the four possible combinations of antenna helicity and background field direction for both radial density profiles are shown in the Fig. $\boxed{6}$. With a radial density gradient, in a rightward field and RH antenna the power deposition is predominantly leftward. The same deposition profile occurs for a leftward field combined with an LH antenna. For the other two combinations the power deposition is predominantly to the left. The left-right power imbalance around z=0 is 36.5% to 63.5%. For the radially homogeneous plasma no significant preferential power deposition exists, with the left-right imbalance being only 48.1% to 51.9%.

Discussion The measurements on and simulations for MAP show qualitatively the same effect of antenna helicity and magnetic field direction on the discharge direction. We have shown computationally that even in an axially homogeneous plasma a radial density gradient leads to a preferential direction for axial power deposition. However the power deposition becomes symmetric when no radial density gradient is present. An understanding of this phenomenon can be gained by deriving the helicon wave equation for a plasma with a purely radial density gradient. We follow Chen's approach 30

who derives the wave equation for a completely homogeneous plasma. Wave fields are assumed to be sinusoidal in the azimuthal and axial directions, i.e. they are of the form $e^{i(m\phi+kz-\omega t)}$, where ω is the angular frequency of the wave. Since in a helicon plasma the electron currents are far stronger than the displacement currents and the ions are immobile, the relevant Maxwell equations in the frequency domain become

$$\nabla \times \mathbf{E} = i\omega \mathbf{B} \tag{2}$$

$$\nabla \times \mathbf{B} \approx \mu_0 \mathbf{j} \approx -\mu_0 en \mathbf{v}.$$
 (3)

where the incompressible electron fluid has density n and velocity v. The electrons are subject to electric, magnetic, friction and pressure gradient forces such that their momentum equation becomes

$$-i\omega m_e \mathbf{v} = -e\left(\mathbf{E} + \mathbf{v} \times \mathbf{B_0}\right) - m_e \nu \mathbf{v} - \frac{k_b T_e}{n} \nabla n, \quad (4)$$

where B_0 is the background magnetic field, T_e is the electron temperature and ν is an effective combined electron-ion and electron-neutral collision frequency.

Utilizing this set of equations we can eliminate E, j and v and arrive for purely radial density gradients at

$$\delta \nabla \times \nabla \times \boldsymbol{B} \mp k \nabla \times \boldsymbol{B} + k_w^2 \boldsymbol{B}$$
$$= \delta \frac{\nabla n}{n} \times (\nabla \times \boldsymbol{B}) \mp i \left(\frac{\nabla n}{n} \cdot (\nabla \times \boldsymbol{B}) \right) \hat{\boldsymbol{z}}, \quad (5)$$

where we have used the definitions

$$\delta = \frac{(\omega + i\nu)m_e}{eB_0} \quad \text{and} \quad k_w^2 = \frac{\omega n\mu_0 e}{B_0}.$$
 (6)

In Eq. 5 the \mp signs account for pointing of the background magnetic field either along or against \hat{z} . The left side of Eq. 5 is the helicon wave equation in a homogeneous plasma as derived in 30. The right side represents a new term which only exists in the presence of a density gradient. We will hereafter refer to this term as the modulating magnetic field as explained below. Since δ is the ratio of the RF frequency to the electron cyclotron frequency, the first term on the right-hand side of Eq. 5 is negligible and the modulating magnetic field becomes

$$\mp i \left(\frac{\nabla n}{n} \cdot (\nabla \times \boldsymbol{B}) \right) \hat{\boldsymbol{z}} \approx \pm \frac{mB_z}{nr} \frac{\partial n}{\partial r} \hat{\boldsymbol{z}}, \tag{7}$$

where the right-hand side exploits that r becomes small towards the plasma core where the density is highest such that the B_z term of $\nabla \times B$ dominates.

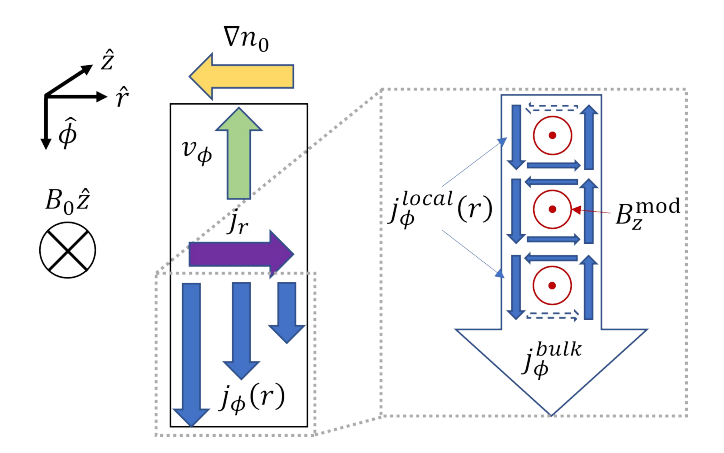


FIG. 7. Mechanism of the shear current source in the presence of a radial density gradient.

This form shows very clearly a dependence on the magnetic field direction, density gradient and azimuthal mode number. In a background field aligned with \hat{z} the additional modulating magnetic field enhances positive but attenuates negative m modes. Together with the fact that antennas of opposite helicity send those modes in opposite directions this explains the dominance of right-handed over left-handed modes, the directionality of helicon discharges and why helicity or field reversal flip the discharge direction.

The physical mechanism behind this effect can be understood by using Eq. 3 to bring the wave equation into the form

$$\delta \nabla \times \nabla \times \boldsymbol{B} \mp k \nabla \times \boldsymbol{B} + k_w^2 \boldsymbol{B} = \mp \frac{i\mu_0}{n} \frac{\partial n}{\partial r} j_r \hat{\boldsymbol{z}}, \quad (8)$$

which shows that the radial currents in conjunction with the field direction and density gradient are responsible for the additional modulating magnetic field which has a $\mp 90^{\circ}$ phase shift to the j_r wave currents.

An physical explanation of this phenomenon is given in Fig. $\boxed{7}$ In a background field along \hat{z} an electron fluid element carrying a radial current j_r is subject to a Lorentz force resulting in a current in the azimuthal direction. This current experiences a Lorentz force as well, resulting in a current in the negative radial direction. This is the mechanism by which helicon waves exchange energy between radial and azimuthal currents in a homogeneous plasma. However, in the presence of an electron density gradient neighboring fluid elements will carry azimuthal currents with magnitudes proportional to the electron density, leading to an azimuthal shear current. These currents can be described by a bulk current plus local currents for the different radial positions. The local parts represent dipole currents

which create a magnetic field in the $\pm \hat{z}$ direction which we have expressed mathematically by the modulating magnetic field in Eq. 8 For an RH helicon mode in a homogeneous plasma the j_r currents lead j_ϕ by 90° such that the modulating field points along the wave's regular B_z field and leads to an enhancement of the wavefields. In contrast an LH mode has j_r lagging j_ϕ by 90° such that the additional modulating magnetic field results in B_z wavefields in the wrong direction, thereby attenuating j_r , j_ϕ and the wave overall.

This effect is visible in simulations as shown in Fig. 8 for the leading RH and LH modes in an axially uniform plasma with radial density gradient. For the RH mode the wavefields are enhanced as evidenced by increased amplitudes of j_r , j_ϕ and B_z where the additional modulating magnetic field is strong. For the LH mode the B_z field is increased where the modulating field is strong but it points in the wrong direction, leading to a reduction of j_r , j_ϕ and the LH wave overall.

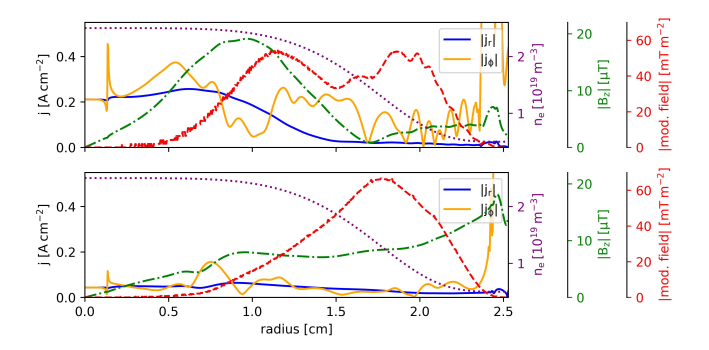


FIG. 8. Wave magnetic fields, currents, modulating field strength and density over radius for RH (top) and LH (bottom) modes.

The modulating magnetic field results in a distortion of the RH and LH magnetic wave field lines compared to those in a homogeneous helicon plasma. demonstrated in Fig. 9 which shows cross sections of the RH (left) and LH (right) mode magnetic wave fields at the some axial locations as in Fig. 8 superimposed on the magnitude of the modulating field. The enhancement of the RH mode is visible by a lack of the vortices that are normally present in RH modes 34 in addition to a general dragging of the field lines in the direction of rotation of the RH mode, i.e. in this view counterclockwise. For the LH mode the strength of vortices is increased and we find regions of field reversal at the radial locations with strong modulation fields. Fields line are dragged counterclockwise as well which is against the direction of rotation for the LH mode.

Summary We have shown experimentally, computationally and analytically that azimuthal shear currents

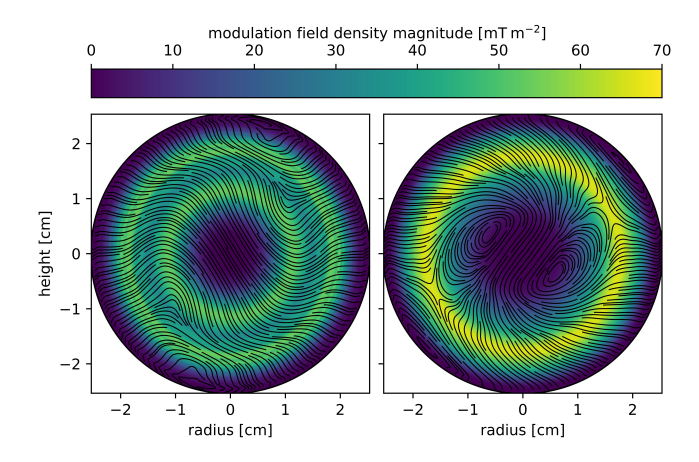


FIG. 9. Magnitude of the additional modulating magnetic field and wave magnetic fields lines for RH (left) and LH (right) modes

induced by radial density gradients are responsible for the directionality of helicon plasmas through an enhancement of right-handed and attenuation of lefthanded modes. This explains long standing observations of discharge directionality and preferential excitation of right-handed modes in helicon plasmas. The discharge direction is defined by the combination of antenna helicity and magnetic background field direction. Lefthanded and right-handed half-helical antennas as well as opposite field directions produce identical discharges with the only difference being an axial mirroring around the antenna location. The shear currents generate a magnetic field which modulates the wave magnetic fields in the axial direction. The opposite phasing of currents in right-handed and left-handed helicon modes results in the modulating field amplifying right-handed but attenuating left-handed modes which leads to the observed directionality of helicon discharges. half-helical antennas of opposite helicity send righthanded and left-handed modes in opposite directions the directionality is reversed when the antenna helicity is changed. Further, since right- or left-handedness of a mode with a given spatial rotation direction depends on the direction of the background field the discharge is reversed when the field direction is reversed.

Acknowledgements This work was funded by the National Science Foundation under grant PHY-1903316 and NSF-CAREER award PHY-1455210 as well as support by the College of Engineering at UW-Madison.

^{*} granetzny@wisc.edu

^[1] R. W. Boswell, Plasma Physics and Controlled Fusion **26**, 1147 (1984)

- [2] F. F. Chen, Plasma Physics and Controlled Fusion 33, 339 (1991).
- [3] J. A. Lehane and P. C. Thonemann, Proceedings of the Physical Society 85, 301 (1965).
- [4] L. C. Woods, Journal of Fluid Mechanics 13, 570 (1962)
- [5] J. P. Klozenberg, B. Mcnamara, and P. C. Thonemann, Journal of Fluid Mechanics 21, 545 (1965)
- [6] P. Aigrain, in Intl. Conf. on Semiconductor Physics (1960) p. 224.
- [7] B. Buttenschön, N. Fahrenkamp, and O. Grulke, Plasma Physics and Controlled Fusion 60, 10.1088/1361-6587/aac13a (2018).
- [8] G. R. Tynan, A. D. Bailey, G. A. Campbell, R. Charatan, A. de Chambrier, G. Gibson, D. J. Hemker, K. Jones, A. Kuthi, C. Lee, T. Shoji, and M. Wilcoxson, Journal of Vacuum Science & Technology A: Vacuum, Surfaces, and Films 15, 2885 (1997).
- [9] J. P. Squire, F. R. Chang-Díaz, T. W. Glover, V. T. Jacobson, G. E. McCaskill, D. S. Winter, F. W. Baity, M. D. Carter, and R. H. Goulding, Thin Solid Films 506-507, 579 (2006).
- [10] J. Rapp, T. M. Biewer, T. S. Bigelow, J. B. Caughman, R. C. Duckworth, R. J. Ellis, D. R. Giuliano, R. H. Goulding, D. L. Hillis, R. H. Howard, T. L. Lessard, J. D. Lore, A. Lumsdaine, E. J. Martin, W. D. McGinnis, S. J. Meitner, L. W. Owen, H. B. Ray, G. C. Shaw, and V. K. Varma, IEEE Transactions on Plasma Science 44, 3456 (2016).
- [11] J. Rapp, T. M. Biewer, T. S. Bigelow, J. F. Caneses, J. B. Caughman, S. J. Diem, R. H. Goulding, R. C. Isler, A. Lumsdaine, C. J. Beers, T. Bjorholm, C. Bradley, J. M. Canik, D. Donovan, R. C. Duckworth, R. J. Ellis, V. Graves, D. Giuliano, D. L. Green, D. L. Hillis, R. H. Howard, N. Kafle, Y. Katoh, A. Lasa, T. Lessard, E. H. Martin, S. J. Meitner, G. N. Luo, W. D. McGinnis, L. W. Owen, H. B. Ray, G. C. Shaw, M. Showers, and V. Varma, Nuclear Fusion 57, 10.1088/1741-4326/aa7b1c (2017).
- [12] T. Watari, T. Hatori, R. Kumazawa, S. Hidekuma, T. Aoki, T. Kawamoto, M. Inutake, S. Hiroe, A. Nishizawa, K. Adati, T. Sato, T. Watanabe, H. Obayashi, and K. Takayama, Physics of Fluids 21, 2076 (1978).

- [13] D. G. Miljak and F. F. Chen, Plasma Sources Science and Technology 7, 61 (1998).
- [14] I. D. Sudit and F. F. Chen, Plasma Sources Science and Technology 5, 43 (1996).
- [15] F. F. Chen, Plasma Sources Science and Technology 24, 10.1088/0963-0252/24/1/014001 (2015).
- [16] S. Shinohara and T. Tanikawa, Review of Scientific Instruments 75, 1941 (2004)
- [17] J. Green and O. Schmitz, Plasma Sources Science and Technology 29, 10.1088/1361-6595/ab7852 (2020).
- [18] S. C. Thakur, C. Brandt, L. Cui, J. J. Gosselin, and G. R. Tynan, IEEE Transactions on Plasma Science 43, 2754 (2015).
- [19] R. F. Boivin, J. L. Kline, and E. E. Scime, Physics of Plasmas 8, 5303 (2001).
- [20] D. D. Blackwell and F. F. Chen, Plasma Sources Science and Technology 6, 569 (1997).
- [21] A. W. Degeling, C. O. Jung, R. W. Boswell, and A. R. Ellingboe, Physics of Plasmas 3, 2788 (1996)
- [22] Y. T. Sung, Y. Li, and J. E. Scharer, Physics of Plasmas 23, 1 (2016).
- [23] R. M. Magee, M. E. Galante, J. Carr, G. Lusk, D. W. McCarren, and E. E. Scime, Physics of Plasmas 20, 1 (2013).
- [24] K. K. Chi, T. E. Sheridan, and R. W. Boswell, Plasma Sources Science and Technology 8, 421 (1999).
- [25] M. M. Balkey, R. Boivin, J. L. Kline, and E. E. Scime, Plasma Sources Science and Technology 10, 284 (2001)
- [26] M. Afsharmanesh and M. Habibi, Review of Scientific Instruments 89, 10.1063/1.5010010 (2018).
- [27] P. A. Piotrowicz, J. F. Caneses, D. L. Green, R. H. Goulding, C. Lau, J. B. Caughman, J. Rapp, and D. N. Ruzic, Plasma Sources Science and Technology 27, 10.1088/1361-6595/aabd62 (2018).
- [28] P. Guittienne, E. Chevalier, and C. Hollenstein, Journal of Applied Physics 98, 10.1063/1.2081107 (2005).
- [29] J. Green, O. Schmitz, and M. Zepp, Physics of Plasmas 27, 043511 (2020).
- [30] F. F. Chen and D. Arnush, Physics of Plasmas 4, 3411 (1997).
- [31] D. Arnush, Physics of Plasmas 7, 3042 (2000)
- [32] F. F. Chen and D. D. Blackwell, Phys. Rev. Lett. 82, 2677 (1999).
- [33] D. Arnush and F. F. Chen, Physics of Plasmas 5, 1239 (1998)
- [34] F. F. Chen, Physics of Plasmas 3, 1783 (1996).